

Searching for large scale structure in deep radio surveys

Audra Baleisis,^{1,3} Ofer Lahav,^{1,4} Andrew J. Loan,¹ and Jasper V. Wall²

¹ *Institute of Astronomy, Madingley Road, Cambridge, CB3 0HA*

² *Royal Greenwich Observatory, Madingley Road, Cambridge, CB3 0EZ*

³ *University of Arizona, Steward Observatory, Tucson, AZ 85721, U.S.A.*

⁴ *Anglo-Australian Observatory, P.O. Box 296, Epping, NSW 2121, Australia*

10 June 2021

ABSTRACT

We calculate the expected amplitude of the dipole and higher spherical harmonics in the angular distribution of radio galaxies. The median redshift of radio sources in existing catalogues is $z \sim 1$, which allows us to study large scale structure on scales between those accessible to present optical and infrared surveys, and that of the Cosmic Microwave Background (CMB). The dipole is due to 2 effects which turn out to be of comparable magnitude: (i) our motion with respect to the CMB, and (ii) large scale structure, parameterised here by a family of Cold Dark Matter power-spectra. We make specific predictions for the Green Bank 1987 (87GB) and Parkes-MIT-NRAO (PMN) catalogues, which in our combined catalogue include $\sim 40,000$ sources brighter than 50 mJy at 4.85 GHz, over about 70% of the sky. For these relatively sparse catalogues both the motion and large scale structure dipole effects are expected to be smaller than the Poisson shot-noise. However, we detect dipole and higher harmonics in the combined $87GB - PMN_{raw}$ catalogue which are far larger than expected. We attribute this to a 2% flux mismatch between the two catalogues. Ad-hoc corrections to match the catalogues may suggest a marginal detection of a dipole. To detect a dipole and higher harmonics unambiguously, a catalogue with full sky coverage and $\sim 10^6$ sources is required. We also investigate the existence and extent of the Supergalactic Plane in the above catalogues. In a strip of $\pm 10^\circ$ of the standard Supergalactic equator, we find a 3σ detection in PMN_{raw} , but only 1σ in $87GB_{raw}$. We briefly discuss the implications of on-going surveys such as FIRST and NVSS and follow up redshift surveys.

Key words: galaxies: large scale structure – radio galaxies – dipole – spherical harmonics – etc.

1 INTRODUCTION

Our local universe is overwhelmingly clumpy. As we look on increasingly larger scales, we continue to see clustering. Observations of discrete objects and their clustering properties on $\sim 100 h^{-1}$ Mpc scales start to show evidence for homogeneity. The largest scales we observe ($\sim 1000 h^{-1}$ Mpc) are by looking at the Cosmic Microwave Background (CMB). In the CMB (apart from a dipole component attributed to our motion) we see a striking level of isotropy, with fluctuations at the level of 10^{-5} on 10° scales (Smoot et al. 1992). Somewhere between the scale accessible to us by the CMB and that of galaxies and quasars, the universe changed from smooth to lumpy, forming structures from some small initial fluctuations.

It has been suggested (Kaiser 1984) that galaxies form preferentially in high density peaks of the underlying mass distribution. If this is true, then the statistics of galaxy dis-

tributions provide us with information, albeit biased, about the underlying dark matter distribution.

Optical and infrared galaxy surveys have been used extensively to study clustering out to $\sim 200 h^{-1}$ Mpc, or a redshift of $z \sim .07$ (e.g. Strauss & Willick 1995 for review). The high luminosity of radio galaxies and quasars, makes them detectable out to large, cosmological distances ($z \sim 4$) and consequently, useful in studying clustering out to high redshift. Unfortunately, most large surveys to date provide only fluxes and angular coordinates on the sky, not redshifts, for individual objects. This means that at present, only the projected distributions of radio galaxies can be studied.

It has long been debated whether radio galaxies are clustered or isotropic on the largest scales. The much quoted study by Webster (1976), which looked at 8000 radio sources at 408 MHz, found $< 3\%$ variability in the number of sources found in a randomly placed 1 Gpc cube. This led to the generally accepted view that radio sources were isotropically

arXiv:astro-ph/9709205v1 22 Sep 1997

distributed. Even if this were not true, the large range in intrinsic luminosities of radio sources would effectively wash out structures when the distribution was projected onto the sky and information about the objects' radial distribution was lost. More recently, Shaver & Pierre (1989) reported a detection of slight clustering of bright, nearby radio sources to the Super Galactic Plane (SGP) and Benn & Wall (1995) discussed other measures of anisotropy in radio surveys. In Section 7 we investigate the presence of the SGP in the $87GB_{raw}$ and PMN_{raw} and report on marginal detection. Clustering in the above catalogues was also studied by correlation function analysis (Kooiman, Burns & Klypin 1995; Sicotte 1995; Loan, Wall & Lahav 1997). These studies indicated that radio galaxies are actually more strongly clustered than local optical galaxies. This conclusion is also confirmed by correlation analysis of the FIRST survey (Cress et al. 1997). Motivated by these recent indicators of clustering in radio surveys and by the upcoming deeper surveys such as FIRST and NVSS (see Condon 1997 for review), we attempt here to study large scale structure in radio surveys using Spherical Harmonic Analysis (SHA).

At this point, we introduce the labels that we use to refer to various forms of the 87GB and PMN catalogues. From here on, we will distinguish between the raw, uncorrected, combined catalogue ($87GB - PMN_{raw}$), and our \mathcal{N} matched (corrected) version of the combined catalogue ($87GB - PMN_{match}$). When talking about predictions, we use the label 87GB-PMN (with no subscripts) to refer to an ideal 4.85 GHz survey.

In Section 2, we present the $87GB_{raw}$ and PMN_{raw} catalogues and discuss their mismatch. In Section 3, we show the formalism of predicted rms harmonics for the models. In Section 4, we look at the radio dipole and how it compares to the predicted dipoles due to shot noise, our motion with respect to the CMB, and large scale structure. In Section 5, we consider the observed dipole in the combined catalogue, and in Section 6, apply the SHA to the catalogue. In Section 7, we discuss the Supergalactic Plane and in Section 8, we summarize the results and discuss future surveys.

2 THE RADIO CATALOGUES

2.1 The Green Bank survey (87GB)

The 87GB survey was carried out by Condon, Broderick & Seielstad (1989), over a period of three years (1986-88), using the NRAO 91m transit radio telescope (in Green Bank, West Virginia, USA) in conjunction with the NRAO 4.85 GHz, 7-beam receiver that was built for the survey. A large part of the sky visible from the Northern Hemisphere was observed ($0^\circ < \delta < +75^\circ$, $0^h < \alpha < 24^h$). Errors due to instrument noise and source confusion for the survey were estimated to be $\sigma \sim 5\text{mJy}$ and a detection threshold of $S \geq 5\sigma$ was adopted in compiling the source lists. A catalogue of 54,579 radio sources above a flux limit of $\sim 25\text{mJy}$ was subsequently produced (Gregory & Condon, 1991) from observations taken in 1987. Excluding a few small regions thought to be contaminated by sidelobes of strong local sources or by solar interference, data from all the surveyed regions were included in the source catalogue, which covers ~ 6 steradians on the sky.

2.2 The Parkes-MIT-NRAO survey (PMN)

The PMN survey was carried out by Griffith & Wright (1993) over the course of 1990, using the Parkes 64m telescope (near Parkes, New South Wales, Australia) in conjunction with the same 7-beam receiver as used in 87GB survey. The area to be surveyed, which covered $-87.5^\circ < \delta < +10.0^\circ$, for all right ascensions ($0^h < \alpha < 24^h$) in the Southern Celestial Hemisphere, was divided and observed in 4 declination strips (see Table 1, Griffith & Wright 1993). The source detection reliability criterion was 90%, corresponding to about $S \geq 4.4\sigma$. The definition adopted of a real source, was that its observed flux was close to the flux limit - not necessarily above the flux limit. Source catalogues for three of the four declination strips have been compiled (Tropical - by Griffith et al. 1994; Southern - by Wright et al. 1994 and independently by Gregory et al. 1994; Equatorial - by Griffith et al. 1995), together covering ~ 6.4 steradians of sky. More recently, the source catalogue for the fourth declination strip (Zenith) has become available (Wright et al. 1996), but because of its lower flux limit of about 72mJy, it is not included in this study.

2.3 How well are the resulting catalogues matched?

We intend to use the $87GB_{raw}$ and PMN_{raw} catalogues together to provide extensive sky coverage, and need some idea of what inconsistencies might arise from the fact that different telescopes were used to collect the data and different reduction algorithms and selection criteria were used in compiling the catalogues. Fortunately, there are two regions of the sky for which there is overlap information.

2.3.1 Region 1

The declination band $0^\circ < \delta < 10^\circ$ was observed with both the NRAO and Parkes telescopes and the data collected reduced by 87GB catalogue method (Gregory & Condon 1991; Gregory et al. 1994) as well as the PMN catalogue method (Griffith et al. 1994; Griffith et al. 1995). Griffith et al. (1995) examine the agreement between resulting catalogues. They find some discrepancies in positions and a 2% disagreement of flux scales. A number of explanations for these inconsistencies are offered:

- Two different telescopes were used to collect the data.
- The observations were carried out at 2 different epochs.
- Different reduction algorithms were used.
- Different source detection thresholds were used.

2.3.2 Region 2

Two catalogues (Gregory et al. 1994; Wright et al. 1994) were produced with data from the PMN survey, Southern declination strip. Gregory et al. (1994) compare the results of two data reduction techniques used to compile the two source lists:

- They find good agreement of positions of strong sources, but up to 1σ disagreement in faint source positions.
- They find the Wright et al. (1994) resulting catalogue contains more sources overall.

2.3.3 Problems within individual catalogues

Two effects cause the flux limit of the 87GB survey to vary with declination, increasing from ~ 25 mJy at $\delta > 60^\circ$ to ~ 40 mJy at $\delta = 0^\circ$ (Gregory & Condon 1991). One is the elevation dependence of the sensitivity of the 91 m NRAO telescope, caused by a higher noise level at larger angles from the local zenith ($\delta = 38^\circ$). The other is the fact that adjacent observing tracks are spaced slightly further apart with decreasing declination. The Parkes telescope does not suffer decreased sensitivity at low elevations. However, the declination-dependent track spacing holds for low declinations ($\delta < -70^\circ$) and causes the flux limit to decrease from ~ 50 mJy near the zenith to ~ 40 mJy near the pole.

2.3.4 What we use as our catalogue

We use the same cuts of the source catalogues as listed in Table 1 in Loan et al. (1997), resulting in sky coverage of $\sim 70\%$. We impose a working lower flux limit of 50 mJy. Figure 1 shows the distribution of the raw data over the sky, in equatorial coordinates. Here we discuss the procedure used to try correcting for the flux and number discrepancies mentioned in the discussion of the overlapping regions above. A measurement of \mathcal{N} for each catalogue separately, at a given flux cutoff, shows that $\mathcal{N}_{PMN-raw} > \mathcal{N}_{87GB-raw}$ by a few percent for the range of flux cutoffs considered above as listed in columns 1-4 of Table 1. It is possible that we are detecting actual large scale structure on the scale of the catalogues, but it is more likely that the inconsistencies (discussed in Section 2) in the methods by which catalogues were compiled are responsible.

In an attempt to correct for the incompatibility of the two catalogues, we chose the following procedure to set $\mathcal{N}_{PMN} \approx \mathcal{N}_{87GB}$: Mean density (\mathcal{N}) matching - We take 87GB fluxes as fiducial. For each flux cutoff (and corresponding \mathcal{N}) in the 87GB_{raw} catalogue, we find the flux cutoff in the PMN_{raw} catalogue that gives \mathcal{N}_{PMN} as close as possible to \mathcal{N}_{87GB} . Columns 1, 2, and 5-7 in Table 1 list these values. The numbers are not perfectly matched as the fluxes are quantized in units of 1mJy. The 60 mJy is the worst matched.

3 SPHERICAL HARMONIC ANALYSIS

It is common (e.g. Peebles 1980) to express the overdensity at a given point as a superposition of Fourier modes $\delta_{\mathbf{k}}$:

$$\delta(\mathbf{r}) \equiv \frac{\delta\rho}{\rho}(\mathbf{r}) = \frac{1}{(2\pi)^3} \int d^3k \delta_{\mathbf{k}} e^{-i\mathbf{k}\cdot\mathbf{r}}, \quad (1)$$

where \mathbf{r} refers to comoving coordinates. In linear theory ($\delta(\mathbf{r}) \ll 1$), the perturbation corresponding to a given wavenumber, \mathbf{k} , is assumed to evolve independently of all other \mathbf{k} modes.

An alternative presentation of power on different scales is by Spherical Harmonic Analysis (SHA), which has become popular in recent years in studying the CMB and galaxy surveys. The idea of using SHA to study galaxy distributions was first proposed over 20 years ago (Peebles 1973). The successful application of this method to actual data had to wait another decade for galaxy surveys (e.g. IRAS) that

covered enough of the sky and contained enough objects to make SHA feasible. Unfortunately, for most of the objects detected, no redshifts were available. In this case, the true 3D galaxy distribution is seen projected onto the surface of the celestial sphere and the spherical harmonic analysis is done in 2D (Scharf et al. 1992, Lahav 1994). When redshifts became available, the spherical harmonic analysis formalism was extended to 3D (Scharf & Lahav 1993; Fisher, Scharf & Lahav 1994; Fisher et al. 1995a; Heavens & Taylor 1995; Nusser & Davis 1994). In the 3D case, the redshift distortion introduced by individual galaxies' peculiar velocities must be corrected for in order to get distance information. As the radio catalogues described here provide only the angular position of galaxies, we consider here 2D harmonic formalism, but relate it to the 3D power-spectrum.

3.1 2D Harmonic Formalism

Expanding a galaxy distribution in terms of spherical harmonic order, l , gives us information about clustering amplitude as a function of angular scale, $\Delta\theta \sim \frac{\pi}{l}$, on the sky. This angular scale can be related to a linear scale by incorporating distance information in the form of either individual galaxy redshifts or overall redshift distribution, $N(z)$, of the galaxies.

The distribution is expanded in spherical harmonics:

$$\sigma(\hat{\mathbf{r}}) = \sum_{l,m} a_l^m Y_l^m(\hat{\mathbf{r}}), \quad (2)$$

where $\hat{\mathbf{r}}$ is the angular position on the sky, and the resulting harmonic coefficients are

$$a_l^m = \sum_{i=1}^N Y_l^{m*}(\hat{\mathbf{r}}_i). \quad (3)$$

In the case of incomplete sky coverage we derive the harmonic coefficients from the data as

$$c_{l,obs}^m = \sum_{i=1}^{N_{gal}} Y_l^{m*}(\hat{\mathbf{r}}_i) - \mathcal{N} \int_{\Omega_{obs}} d\Omega Y_l^{m*}(\Omega), \quad (4)$$

where \mathcal{N} is the number of sources per steradian. The first term on the right hand side is a_l^m from eqn. 3, and the second term is the correction for the unsurveyed and excluded regions of the sky. The second term (calculated by Monte Carlo integration) is included so that, for a Poisson distribution of galaxies, $c_{l,obs}^m = 0$ (for $l > 0$) when $N_{gal} \rightarrow \infty$.

3.2 Predicted Harmonics

We can predict what the above a_l^m should be, for a given cosmology and power spectrum of fluctuations, $P(k)$ (dictated by a dark matter model). Note that the 2D spherical harmonic analysis formalism can be extended to other cosmologies (Langlois et al, in preparation), but for this discussion we assume an Einstein-de Sitter universe ($\Omega = 1, \Lambda = 0$).

We also account for the fact that a galaxy survey will only detect a fraction of the radio galaxies that populate the surveyed volume by including the selection function, $\Phi(r)$, which is the probability that a radio galaxy will be detected at distance r in this flux limited survey. The observed galaxy distribution is expanded in summation because galaxies are

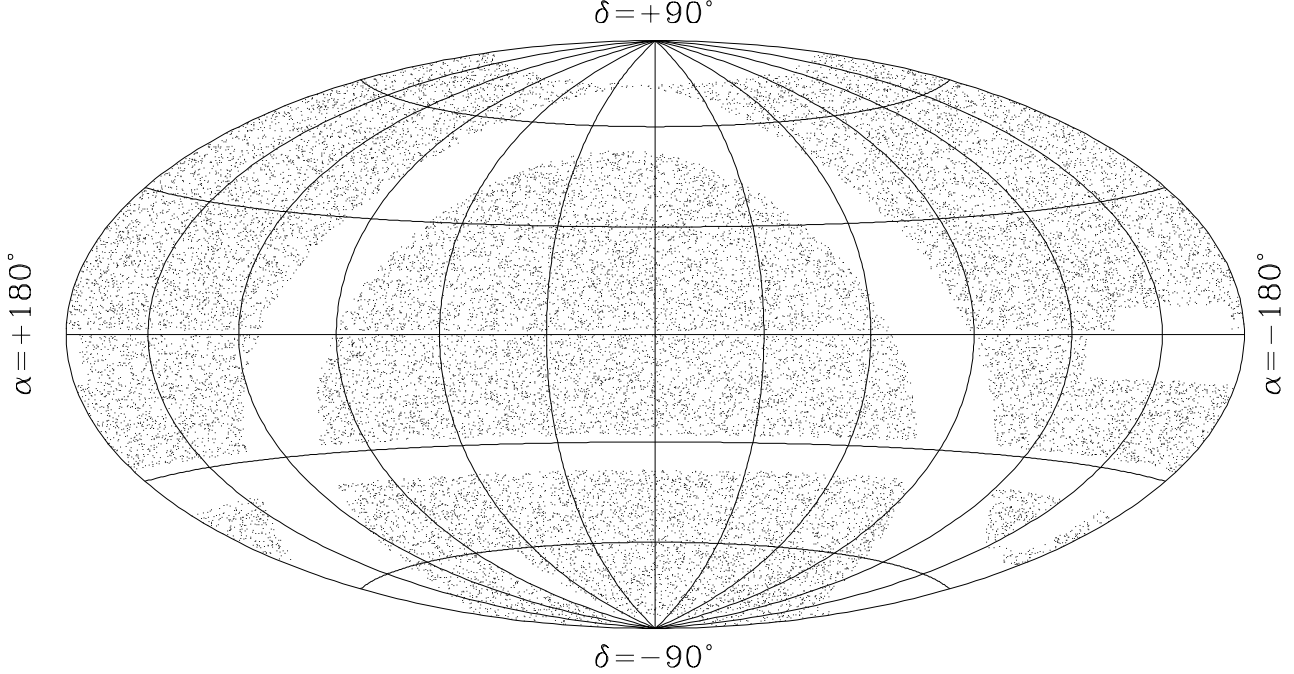


Figure 1. The distribution of radio sources (above flux cutoff of 70mJy in $87GB_{raw}$, 74 mJy in PMN_{raw}) from the $87GB - PMN_{raw}$ catalogue areas as selected by Loan et al. 1997. This is an Aitoff projection in Equatorial coordinates.

Table 1. Results of mean density (\mathcal{N}) matching procedure. The columns labeled % dif. give the percentage by which the larger \mathcal{N} exceeds the smaller \mathcal{N} .

S_{lim}	$\mathcal{N}_{87GB-raw}$	$\mathcal{N}_{PMN-raw}$	% dif.	S_{lim}	$\mathcal{N}_{PMN-match}$	% dif.
50	4457	4929	10.5 %	54	4433	0.5 %
60	3520	3836	8.9 %	61	3744	6.4 %
70	2870	3123	8.8 %	74	2891	0.7 %
80	2386	2616	9.6 %	85	2403	0.7 %
90	2021	2241	10.8 %	97	2012	0.4 %
100	1751	1922	9.8 %	107	1758	0.4 %
200	655	684	4.4 %	205	658	0.5 %

discrete objects. To model the underlying mass distribution, which is continuous, the expansion is in integral form. Here we follow the formalism developed by Lahav, Piran & Treyer (1997) for the X-ray Background. As the sources of the X-ray Background are not resolved, the sources are flux weighted in their formalism. In our case, weighting by the flux of each radio source can make the measurements very noisy. Instead, we derive here the number weighted case (cf. Piran & Singh 1996 for a similar formalism for Gamma-ray bursts). We begin by writing the harmonics as

$$a_l^m = \int dV_c [1 + b_R \delta_m(\mathbf{r})] \Phi(r) Y_l^{m*}(\hat{\mathbf{r}}), \quad (5)$$

and the *fluctuations* over the mean in the distribution (for $l > 0$) as

$$a_l^m = \int d\omega dr r^2 \delta_R(\mathbf{r}) \Phi(r) Y_l^{m*}(\hat{\mathbf{r}}), \quad (6)$$

where the comoving volume element dV_c has been split into its radial and angular components, and δ_R is the fluctuation in the number of radio galaxies with respect to the mean.

For simplicity (reflecting our ignorance about the evolution of radio sources) we have assumed linear epoch-independent biasing factor between the radio sources and the mass fluctuations

$$\delta_R(\mathbf{r}) = b_R \delta_m(\mathbf{r}). \quad (7)$$

Now we make use of the Fourier relation between the spatial and wavenumber density fluctuations. By substituting the Rayleigh expression,

$$e^{i\mathbf{k}\cdot\mathbf{r}} = 4\pi \sum_{lm} i^l j_l(kr) Y_l^{m*}(\hat{\mathbf{r}}) Y_l^m(\hat{\mathbf{k}}), \quad (8)$$

into eqn. 1, it becomes

$$\delta(\mathbf{r}) = \frac{1}{2\pi^2} \sum_{lm} (i^l)^* Y_l^m(\hat{\mathbf{r}}) \int d^3k \delta_{\mathbf{k}}(z) Y_l^{m*}(\hat{\mathbf{k}}) j_l(kr). \quad (9)$$

By substituting this expression for the density fluctuation term in eqn. 6, we get

$$a_l^m = \frac{b_R}{2\pi^2} \int \int d\omega dr r^2 \Phi(r) \sum_{l',m'} (i^{l'})^* Y_l^m(\hat{\mathbf{r}}) Y_{l'}^{m'*}(\hat{\mathbf{r}})$$

$$\times \int d^3k \delta_{\mathbf{k}}(z) Y_l^{m'*}(\hat{\mathbf{k}}) j_l'(kr). \quad (10)$$

By the orthogonality relation, $\int d\omega Y_l^m(\hat{\mathbf{r}}) Y_l^{m'*}(\hat{\mathbf{r}}) = \delta_{ll'}^{mm'}$ (where $\delta_{ll'}^{mm'}$ is the Kronecker delta function), the \sum over l and m drops out of the above expression.

Mass density fluctuations evolve with time, growing as the scale factor

$$\delta_{\mathbf{k}}(z) = \delta_{\mathbf{k}}(0) (1+z)^{-\mu}. \quad (11)$$

In linear theory $\mu = 1$ for an Einstein-de Sitter universe, and from here on we adopt this value.

We take the mean square of the a_l^m 's and then the ensemble average of the result. We use the definition below to rewrite the density fluctuation term $\langle \delta_{\mathbf{k}} \delta_{\mathbf{k}'}^* \rangle$ as:

$$\langle \delta_{\mathbf{k}} \delta_{\mathbf{k}'}^* \rangle = (2\pi)^3 P(k) \delta^{(3)}(\mathbf{k} - \mathbf{k}'), \quad (12)$$

where $P(k)$ is the power spectrum of fluctuations in mass and $\delta^{(3)}$ is the 3-dimensional Dirac delta function.

After grouping some of the terms into the window function, $\Psi_l(k)$, we have

$$\langle |a_l^m|^2 \rangle = \frac{2}{\pi} b_R^2 \int dk k^2 P(k) |\Psi_l(k)|^2. \quad (13)$$

The expression we evaluate now gives the ensemble average (in the rms sense) harmonic coefficients. This is the prediction for the harmonic coefficients we would get if we averaged the a_l^m 's measured by all possible observers (under the same observational conditions we have) in the universe. Of course, the radio data represent only one realization, but for each harmonic l , we have $(2l+1)$ independent measurements.

To model the fluctuations we parametrize $P(k)$ for a family of Cold Dark Matter (CDM) models. In this case the shape of $P(k)$ is determined by the product of the density parameter and the Hubble constant $\Gamma \equiv \Omega h$. This parameter is related to the size of the horizon when the densities of matter and radiation were equal. For standard CDM $\Gamma = 0.5$, while for low density CDM model which fits empirically clustering of APM and IRAS galaxies, $\Gamma = 0.2$. A smaller Γ gives more power on large scales. The normalization of the mass power spectrum is commonly given by $\sigma_{8,M}$, the rms fluctuations in spheres of $8 h^{-1}$ Mpc.

3.2.1 The Window Function, $\Psi_l(k)$

We have grouped the distance and redshift terms into $\Psi_l(k)$

$$\Psi_l(k) = \int dr r^2 \Phi(r) j_l(kr) (1+z)^{-\mu}. \quad (14)$$

Here r is the comoving distance, which is related to redshift by $r = \frac{2c}{H_0} [1 - (1+z)^{-1/2}]$. We do not know the selection function, $\Phi(r)$, explicitly and have to express in terms of the observed redshift distribution. Radio luminosity functions (Dunlop & Peacock 1990) can be used to calculate the number of radio sources we expect to detect as a function of redshift, z , given the frequency at which we are observing and a flux cutoff. The resulting redshift distribution, $N(z)$, gives the number of radio galaxies observed per steradian at a redshift, z .

$N(z)$ was derived from the Dunlop & Peacock (1990) radio luminosity functions for a number of flux cutoffs, as

explained in Loan et al. (1997). The luminosity range of radio galaxies is so large that the resulting redshift range probed is approximately the same for a range of flux cutoffs.

From the definitions of $\Phi(r)$ and $N(z)$, we know that

$$\int dr r^2 \Phi(r) = \mathcal{N} = \int dz B N(z), \quad (15)$$

where \mathcal{N} is the number of galaxies per steradian in our survey and B is a normalisation constant. Since the above equality holds for all r , we can rewrite $\Psi_l(k)$ in terms of $N(z)$.

$$\Psi_l(k) = 2BQ \int dx N(z(x)) j_l(x) (1-Qx)^{-1}, \quad (16)$$

where we have set $x = kr$ and $Q = H_0/2kc$.

It is very insightful to plot the window function on top of the curves for $k^3 P(k)/(2\pi^2) \sim (\frac{\delta\rho}{\rho})^2$, as it shows what scales of k are probed by particular statistic applied to a specific catalogue. The window function for the quadrupole $|\psi_2(k)|^2$ (eqn. 14) for 70 mJy survey, is shown by the dashed-dotted line in Figure 2, together with the power-spectra for standard CDM (with shape parameter $\Gamma = 0.5$) and low density CDM ($\Gamma = 0.2$) models. In both cases we assume normalization $\sigma_{8,M} = 1$ and $b_R = 1$ (no biasing). The figure illustrates that radio surveys can serve as probes of scales $k_*^{-1} \sim 600h^{-1}$ Mpc, between those accessible to galaxy surveys (e.g. APM) and the CMB (e.g. COBE). Other variants of this plot which include other probes of the power-spectrum (e.g. local redshift surveys and the X-ray Background) are given elsewhere (e.g. Baugh & Efstathiou 1993; Lahav et al. 1997; Wu, Lahav & Rees, in preparation).

3.2.2 Shot Noise

Finally, we need to consider the discreteness of the galaxies, which contributes a shot noise term to the data harmonics. To account for this, we add a shot noise estimate to the predicted model harmonics. Each measured a_l^m will be subject to the same shot noise contamination

$$\langle |a_l^m|^2 \rangle_{SN} = \frac{1}{4\pi} \sum_{sources} 1 = \mathcal{N}, \quad (17)$$

so

$$\langle |a_l^m|^2 \rangle_{tot} = \langle |a_l^m|^2 \rangle_{mod} + \langle |a_l^m|^2 \rangle_{SN}. \quad (18)$$

An added advantage of number weighted harmonics (over flux weighted) comes in here in the shot noise term. For the number weighted case the shot noise is finite, whereas for the flux weighted case it diverges if bright sources are not removed. (cf. Lahav et al. 1997).

3.2.3 Incomplete Sky Coverage

The radio surveys considered here only cover about 70% of the sky. The remaining 30% is filled in approximately uniformly (according to eqn. 4) to the mean density of the surveyed sky. We do this to avoid the crosstalk between the harmonic coefficients, a_l^m , that can result from an incomplete sky. As we mention in Sections 5 and 6, we still measure significantly larger than predicted harmonics amplitudes in the data. However, the SHA formalism presented in Section

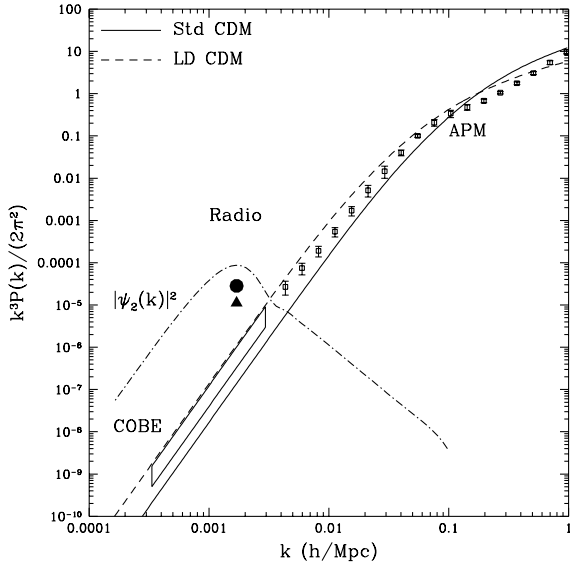


Figure 2. Radio surveys as probes of scales between those accessible to galaxy surveys (e.g. APM) and the CMB (e.g. COBE). The solid and dashed lines represent $k^3 P(k)/(2\pi^2) \sim (\frac{\delta\rho}{\rho})^2$ for standard CDM ($\Gamma = 0.5$) and low density CDM ($\Gamma = 0.2$) models, both normalized with $\sigma_{8,M} = 1$ at $k \sim 0.15$. The open squares at large k 's (small scales) are estimates of the power-spectrum from 3D inversion of the angular APM galaxy catalogue (Baugh & Efstathiou 1993, 1994). The elongated 'box' at small k 's represents the COBE 4-yr CMB measurements (E. Gawiser, private communication). It corresponds to a quadrupole $Q=18.0 \mu K$ for a Harrison-Zeldovich mass power-spectrum, via the Sachs-Wolfe effect, or $\sigma_{8,M} = 1.4$ for a standard CDM model. The dashed-dotted line is the window-function $|\psi_2(k)|^2$ for the quadrupole (eqn. 14) of radio sources brighter than 70 mJy and an Einstein-de Sitter universe. It illustrates the scales probed by the spherical harmonic analysis of radio surveys (eqn. 13). It peaks at $k_*^{-1} \sim 600h^{-1}$ Mpc, indicating the capability of radio surveys to probe intermediate scales. The vertical scaling of the window function is arbitrary. The solid triangle and circle are estimates of the power-spectrum at k_* , assuming the shape of standard CDM and LDCDM power-spectra respectively. They are based on the measured quadrupole from the combined 70 mJy *87GB - PMN_{match}* sample, which correspond to $\sigma_{8,R} = b_R \sigma_{8,M} \sim 9$ and 5 for standard CDM and LDCDM respectively. Given the problems of catalogue matching and shot-noise, these points should be interpreted at best as 'representative upper limits', not as detections.

3 is for full sky coverage. It is possible that despite our treatment of the unsurveyed regions, we are still seeing an effect of incomplete sky coverage.

To make sure that we are comparing the data and model harmonics on equal footing, we want to deal with the unsurveyed sky more rigorously. This can be done in two ways. One is to solve the inversion problem (given the known mask, i.e. unsurveyed region geometry) and to retrieve the data harmonics for a complete sky. The second approach is to adapt the model harmonics to additionally incorporate the effect of incomplete sky coverage and predict the rms harmonics for all observers with the same incomplete sky we have. We use the second method to examine the amplitude of the effect of incomplete sky coverage.

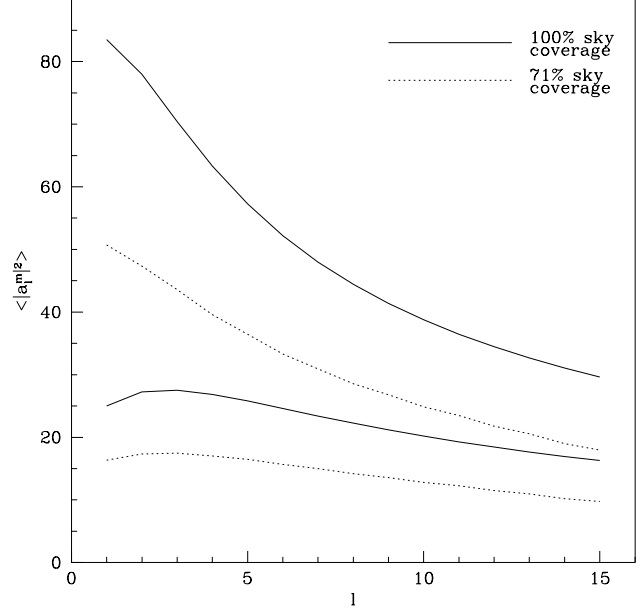


Figure 3. Predicted ensemble average harmonics, using $N(z)$ for a 70 mJy cutoff for LDCDM (higher curve) and CDM (lower curve) power spectra. Solid lines correspond to $\langle |a_l^m|^2 \rangle_{mod}$ for full sky, and dotted lines correspond to $\langle |c_l^m|^2 \rangle_{mod}$ for 70% sky coverage, for an ideal 4.85 GHz survey.

The equation for the predicted harmonics for an incompletely surveyed sky is then

$$\langle |c_l^m|^2 \rangle_{tot} = \sum_{l'} \sum_{m'} |W_{ll'}^{mm'}|^2 \langle |a_{l'}^{m'}|^2 \rangle_{tot}, \quad (19)$$

where the $W_{ll'}^{mm'}$ tensor models the unsurveyed regions (see Peebles 1973, Scharf et al 1992), and the $\langle |a_{l'}^{m'}|^2 \rangle_{tot}$'s are the predicted harmonics for a completely surveyed sky (equation 18). This can also be written as $\langle |c_l^m|^2 \rangle_{tot} = \langle |c_l^m|^2 \rangle_{mod} + \langle |c_l^m|^2 \rangle_{SN}$, where the masked shot-noise term is $\langle |c_l^m|^2 \rangle_{SN} = (\Omega_{obs}/4\pi)\mathcal{N}$.

Details of the calculation of the $W_{ll'}^{mm'}$ tensor are given in Scharf et al (1992), and Zare (1987). The result of this correction is a lowering of the predicted ensemble average amplitudes, not an increase, as might have explained the large observed harmonic amplitudes. The corrected amplitudes $\langle |c_l^m|^2 \rangle_{mod}$ in the absence of shot-noise for a 70 mJy flux cutoff, are shown in Figure 3, compared to the prediction for full sky coverage $\langle |a_l^m|^2 \rangle_{mod}$. This shows the trend in predicted harmonic amplitudes between the CDM and LDCDM power spectra and between full vs. partial sky coverage for a single flux cutoff. There is also a trend across chosen flux cutoff. With respect to the amplitudes shown for a 70 mJy cutoff, those for 50 mJy and 100 mJy are, respectively, $\approx .5\times$ and $\approx 2\times$ as high.

4 THE PREDICTED DIPOLE

The $l = 1$ harmonic term has additional significance in the study of large scale structure. The well known CMB dipole

anisotropy is thought to arise from our peculiar velocity relative to the CMB. This motion is attributed to the gravitational pull of anisotropically distributed mass overdensities around us. In linear theory (Peebles 1980) the peculiar velocity vector, \mathbf{v} , is proportional to the gravitational acceleration vector, \mathbf{g} ,

$$\mathbf{v} \propto \frac{\Omega^{0.6}}{b} \mathbf{g}, \quad (20)$$

where Ω is the density parameter at the present epoch and b is the bias parameter (assuming linear biasing).

Galaxy surveys do not represent the total mass directly, although the light emitted by galaxies at certain frequencies is likely to be indicative of their mass and thus related to the underlying mass distribution. The dipole can be calculated as a flux weighted sum over each galaxy's position (see eqn. 33 for a more general form). If the galaxy's light is proportional to its mass this can represent the gravity vector as both the flux and gravitational force fall off with distance as $1/r^2$.

In practice, however, all available galaxy catalogues are flux limited, and detect only a fraction of the galaxies in any volume surveyed. This means that the calculation will give an estimate of the dipole which is produced by only those galaxies detected out to a limited effective distance. Moreover, in this study, we have fluxes at radio wavelengths and the radio emission from galaxies may not be a good indicator of galaxy mass. We therefore prefer to calculate a number-weighted dipole. As a result, we cannot expect the number-weighted dipole to be aligned with the mass gravity vector and with the CMB Local Group velocity dipole.

We now consider the various effects that may contribute to the dipole amplitude measured for a population of radio sources. We parameterise the dipole as

$$\frac{dN}{d\Omega}(\theta) = \mathcal{N} + A \cos \theta, \quad (21)$$

where the left side of the equation is the mean density of objects measured, per unit solid angle, as a function of direction, θ , on the sky. The angle θ is measured from the direction of peak dipole effect. $\mathcal{N} = \frac{N}{4\pi}$ is the number of galaxies per steradian in the combined 87GB-PMN catalogue for a given flux cutoff. A is the dipole amplitude we expect to measure due to the effects discussed below. The different notation for the dipoles is related as follows:

$$A = \frac{3}{4\pi} D = \frac{3}{\sqrt{4\pi}} \sqrt{\langle |a_1^m|^2 \rangle}, \quad (22)$$

where $D = |\sum_i \hat{\mathbf{r}}_i|$ is the amplitude of the number-weighted dipole calculated and listed in Tables 3 and 4, and $\langle |a_1^m|^2 \rangle$ is the dipole term of the harmonic prediction of our models (Section 3).

As described below, the velocity dipole is a separate effect from the large scale structure dipole, although related to it. The large scale structure induces our motion, which in turn creates the blueshifted excess of galaxies in the direction of motion. The measured dipole will be a combination of these two effects, plus the shot noise contribution.

4.1 Velocity term

For the sake of the following calculation, the population of radio galaxies is assumed to be isotropic in its rest frame.

Ellis and Baldwin (1984) predicted the dipole amplitude we should measure in a flux limited radio galaxy survey, due to our motion with respect to the rest frame of the radio galaxy distribution. Consider a population of radio galaxies, whose radio continua can be characterized by the power law $S \propto \nu^{-\alpha}$, α positive. In the direction of the sun's motion, galaxies are blueshifted, so the observed 4.85 GHz band actually samples a lower frequency band in the rest-frame of the galaxy, and hence a higher flux. The overall effect is that we see more galaxies in the direction of motion and less in the opposite direction than we would if we were not moving with respect to the galaxies' rest frame. This deviation from isotropic number counts introduces a dipole pattern into the galaxy counts. This is similar to the 'Compton-Getting' effect flux dipole due to the motion of the observer relative to a sea of radiation (e.g. the CMB or the X-ray Background).

This velocity dipole effect was predicted by Ellis & Baldwin (1984) as

$$A_{vel} = [2 + x(1 + \alpha)] \frac{v}{c} \mathcal{N}, \quad (23)$$

where x is the slope of the integral source count per unit solid angle, above a given limiting flux, S_{lim} ,

$$\frac{dN}{d\Omega}(S > S_{lim}) \propto S^{-x}. \quad (24)$$

As mentioned above, α is the slope of the power law spectra of the surveyed objects, and v is our velocity with respect to the frame in which the counts are isotropic. Note, that the above estimate is for a number weighted dipole. We take $x = 1$ (= 1.5 in a Euclidean universe), and $\alpha = 0.75$ (mean spectral index of radio galaxy spectra). The velocity inferred from the CMB dipole is $v_{sun-CMB} \sim 370 \frac{km}{s}$. The velocity dipole effect we should measure is

$$A_{vel} = 4.625 \times 10^{-3} \mathcal{N}. \quad (25)$$

As an example of the magnitude of the effect, in the combined catalogue used below we have $\mathcal{N} = 2878$ for $S_{lim} = 70mJy$. In this case:

$$A_{vel} = 13.3 \quad (26)$$

In principle, we can subtract the velocity dipole based on the solar motion with respect to the CMB, and then consider the residual dipole as being purely due to large scale structure. It should be noted that the A_{vel} , unlike A_{LSS} and A_{SN} discussed below, is *not* an rms quantity with zero mean, but in fact a correctable value. It is thus quite different in character from the other two terms. Eq. (23) only holds for a single population of radio sources characterized by spectral index α and counts index x . In reality, the 4.85 GHz sample is composed of different populations, and therefore the expression for A_{vel} should be a superposition due to the different populations. At present the distribution functions for α and x at 4.85 GHz are poorly known, so it is difficult to evaluate the exact prediction for A_{vel} .

At this point, it is important to emphasize the distinction between the two reference frames with respect to which the CMB dipole amplitude and direction are defined. One is the heliocentric frame: $v_{sun-CMB} \sim 370km/s$ towards Galactic coordinates $l = 264^\circ; b = 48^\circ$. As the measurements are done in the heliocentric frame, $v_{sun-CMB}$ will determine the amplitude of A_{vel} . The other relevant reference frame is the Local Group frame: $v_{LG-CMB} \sim 600km/s$

toward $l = 268^\circ; b = 27^\circ$. Since the radio galaxies in the catalogues are outside the Local Group, this pertains to the LSS dipole prediction in our discussion, but as explained above there is no simple relation between a number-weighted dipole and the CMB Local Group velocity dipole.

4.2 Large Scale Structure term

This is the $l = 1$ term, from the predicted spherical harmonics in Section 3.

As an example of the magnitude of the effect we have assumed a power spectrum which fits the observed local clustering of optical and IRAS galaxies, parameterised as an unbiased, low density CDM (hereafter LCDM) power-spectrum with shape parameter $\Gamma = 0.2$. We also assume an Einstein-de Sitter universe ($\Omega = 1$) and hence that fluctuations grow as $(1+z)^{-1}$. We adopt a redshift distribution, $N(z)$, corresponding to a flux cutoff of 70mJy. For these parameters the rms prediction, eqn. 13, gives $\langle |a_1^m|^2 \rangle = 83.52$, which translates into

$$A_{LSS} = 7.7. \quad (27)$$

4.3 Shot Noise term

As mentioned earlier, a shot noise term comes in because we are using discrete galaxies as tracers of a continuous quantity (fluctuations in the mass density). We calculated the Poisson shot noise contribution to be

$$\langle |a_1^m|^2 \rangle_{SN} = \frac{1}{4\pi} \sum_{sources} 1 = \mathcal{N}, \quad (28)$$

so

$$A_{SN} = \frac{3}{\sqrt{4\pi}} \sqrt{\mathcal{N}}. \quad (29)$$

In the case of our combined catalogue for a 70mJy flux cutoff, $\mathcal{N} = 2878$ and we expect:

$$A_{SN} = 45.4. \quad (30)$$

Unfortunately, the shot noise turns out to be the dominant component of any dipole we measure in the 87GB-PMN survey. It is simple to estimate the number of objects we would need to detect the velocity and large scale structure dipoles at the same level as shot noise. For the velocity dipole, we equate eqns. 25 and 29 and find that we need

$$\mathcal{N} \approx 3.35 \times 10^4 \text{ galaxies per str}, \quad (31)$$

which translates into $N \sim 4 \times 10^5$ galaxies over the sky. The large scale structure dipole, A_{LSS} is proportional to \mathcal{N} (see eqns. 13, 15, 16), so by equating eqn. 29 and the expression for the large scale structure dipole we find we need

$$\mathcal{N} \approx 1.06 \times 10^5 \text{ galaxies per str}, \quad (32)$$

(or $N \sim 1.3 \times 10^6$ galaxies total) to be able to detect a large scale dipole (for the LCDM power spectrum, the shape of $N(z)$ and the other parameters mentioned above).

The predicted velocity, large scale structure, and shot-noise dipole effects (for the example parameters mentioned above) are summarized in Table 2. Our a priori calculation shows that we are unlikely to detect a dipole (and higher harmonics, see below) in the 87GB-PMN catalogues due to the high level of shot-noise expected.

Table 2. The amplitudes of various dipole effects, compared to the number weighted dipole we detect (after the \mathcal{N} matching procedure) in the 87GB – PMN_{match} catalogues, for a 70mJy flux cutoff.

Dipole	A (amplitude)
Velocity	13.3
Large Scale Structure	7.7
Shot Noise	45.4
Detected	73.3

Nevertheless, we have attempted to calculate the dipole and higher harmonics from the catalogues for several reasons: (i) The detection of the angular correlation function (Loan et al. 1997) and the Supergalactic Plane (Section 7) in 87GB_{raw} and PMN_{raw} suggests the existence of large scale structure. (ii) It may well be that our formalism of Gaussian random fields does not fully characterize real structure. (iii) Comparison of the predictions to observations can serve as a consistency check of the validity of the 87GB_{raw} and PMN_{raw} flux calibration. (iv) The application to existing catalogues can serve as a pilot study for future deeper surveys.

As described below, we find that the observed dipole is much higher than expected. We attribute this discrepancy to the flux matching of the catalogues. However, it is interesting that after applying an ad-hoc flux matching procedure we still detect a dipole (see Table 2) larger than predicted. Flux cutoffs of 50mJy and 100mJy result in qualitatively similar results - the detected dipole is still higher than the predicted shot noise, large scale structure and velocity dipoles. The magnitude of this surplus of the detected dipole with respect to the predicted dipoles increases with decreasing flux limit. We discuss the implications for this detection in the next few sections.

5 DIPOLE CALCULATION USING THE COMBINED 87GB – PMN_{MATCH} CATALOGUE

Despite the numerous uncertainties in relating the radiation emitted by galaxies to the underlying mass distribution, angular dipole calculations for a variety of galaxy catalogues (e.g. Meiksin & Davis 1986; Yahil, Walker & Rowan-Robinson 1986; Villumsen & Strauss 1987; Lahav 1987; Harmon, Lahav & Meurs 1987; Lahav, Rowan-Robinson & Lynden-Bell 1988; Plionis 1988; Lynden-Bell, Lahav & Burstein 1989; Kaiser & Lahav 1989; Scharf et al. 1992), have found amazingly good alignment ($10^\circ - 30^\circ$) to the CMB dipole in the Local Group frame. Similar alignment has been detected using IRAS redshift surveys (Rowan-Robinson et al. 1991; Strauss et al. 1992; Webster, Lahav & Fisher 1997) and optical redshift surveys (e.g. Hudson 1993).

The detection of a dipole closely aligned with the CMB dipole, in a number of surveys at various wavelengths, suggests that it is worth calculating the dipole for the radio galaxies in the 87GB-PMN survey. We only have angular coordinates and fluxes. The 87GB-PMN surveys have a me-

Table 3. Initial dipole calculation for $87GB - PMN_{raw}$. S_{min} is the flux cutoff in mJy, \mathcal{N} is the number of galaxies per steradian, D is the amplitude of the dipole, and l and b give the Galactic coordinate direction in which the dipole is pointing.

Cumulative dipole ($w_i = 1$)				
S_{min}	\mathcal{N}	D	l	b
50	4671	1342.3	299°	-21°
70	2985	709.2	297°	-15°
100	1831	468.4	300°	-17°

dian redshift of $z \sim 1$. This is important for the question of convergence of the measured galaxy dipole to the CMB dipole. Above some large enough distance from us, we expect the distribution of galaxies to be homogeneous, and not contribute to the CMB dipole. The 87GB-PMN catalogues are deep enough to probe the convergence of the dipole far beyond the limit set by IRAS and optical surveys.

On the other hand, we do not know how well radio radiation from a galaxy indicates its mass, or how radio galaxies are biased with respect to the underlying mass distribution. In addition, the sparse sampling of the 87GB-PMN surveys may make it difficult to even detect a dipole signal. If we assume an Einstein-de Sitter cosmology, for a 70mJy cutoff there are only ~ 500 galaxies out to $100 h^{-1}$ Mpc and ~ 1500 objects out to $z \sim 0.1$ in the combined radio catalogues.

After filling in the unsurveyed regions of the sky, we calculated the radio galaxy dipole for a range of flux cutoffs in the survey. The general form of the dipole calculation (for a full sky distribution of N galaxies) is

$$\mathbf{D} = \sum_{i=1}^N w_i \hat{r}_i. \quad (33)$$

For a flux weighted dipole, $w_i = f_i$, the flux of galaxy i . We use $w_i = 1$, and calculate the number weighted dipole because, although the flux weighted dipole is the optimal calculation to recover the acceleration vector, it is not always reliable. As mentioned above, only some wavelengths of a galaxy's radiation are good indicators of its mass. If there is no correlation between L_{gal} at a given wavelength and M_{gal} , the flux weighted dipole will not give an estimate of the gravitational pull we are experiencing. In such a case, it is better to use a strictly number weighted dipole. Note that this no longer gives an estimate of \mathbf{g} because it does not incorporate the $1/r^2$ fall off in flux to each galaxy (as with $w_i = f_i$), and as such, is no longer directly comparable to the LG-CMB dipole. The results of our initial calculation are shown in Table 3. As mentioned, no alignment was expected. The measured amplitudes, however, are significantly larger than the number weighted prediction from Section 3.

Note that the above dipole calculations have been done under the assumption that the $87GB_{raw}$ and PMN_{raw} catalogues were produced using similar reduction criteria, and that for each flux cutoff $\mathcal{N}_{PMN-raw} = \mathcal{N}_{87GB-raw}$ (where \mathcal{N} is the number of galaxies per steradian on the sky). As mentioned in Section 2, this is not a valid assumption. For the combination of the $87GB_{raw}$ and PMN_{raw} catalogues that we use, we have found the regions of the sky covered by

Table 4. Recalculated dipole - S_{min} is the flux cutoff in mJy, \mathcal{N} is the average number of galaxies per steradian in the $87GB - PMN_{match}$ catalogues, D is the amplitude of the dipole, and l and b give the direction in which the dipole is pointing in Galactic coordinate.

Cumulative dipole ($w_i = 1$)				
S_{min}	\mathcal{N}	D	l	b
50	4443	415.3	284°	25°
60	3622	742.7	293°	-17°
70	2878	307.2	286°	15°
80	2392	251.7	282°	16°
90	2016	169.2	287°	28°
100	1753	158.4	298°	16°
200	656	45.3	274°	-19°

the PMN_{raw} catalogue to have larger \mathcal{N} values for a given flux cutoff.

The resulting dipole in the flux matched catalogue, for a 70mJy flux cutoff was $D = 307.2$, a significant decrease from the original value. The direction also changed considerably, to $l = 286^\circ, b = 15^\circ$, 21° away from the LG-CMB dipole, 38° away from the Sun-CMB dipole.

It is interesting to note that our derived dipole (Table 4) is closer to the Local Group CMB dipole than to the heliocentric CMB dipole. As previously mentioned, however, not much can be inferred from the alignment between our number-weighted dipole and the LG-CMB dipole. At most, this suggests that the velocity dipole does not dominate the measured dipole.

The decrease in the measured dipole amplitude was encouraging enough to recalculate the dipole for other flux cutoffs. The results for a range of flux cutoffs are shown in Table 4 and Figures 4 and 5. The dipole amplitudes are smaller by a factor of 2 – 3, and show much closer alignment to the CMB dipole than before. For the 60 mJy cutoff, the dipole amplitude is still quite high. We attribute this to the poor flux matching for this flux cutoff which left a number density mismatch comparable to some of the original $\mathcal{N}_{PMN-raw}, \mathcal{N}_{87GB-raw}$ percentage differences at other flux cutoffs.

We see a significant reduction in the amplitude and change in the direction of the dipole, after applying fairly naive (and seemingly small) changes to the catalogues. It is possible that the catalogue geometry (which we have tried to correct for by approximately uniform filling in of the unsurveyed regions) is causing a residual dipole signal.

5.1 Summary and discussion of dipole calculation

For the radio sources in the 4.85 GHz, 87GB-PMN combined catalogue, for a flux cutoff of 70 mJy, we find the following:

- (i) We predict the effects of our motion and of large scale structure to be comparable in amplitude to within a factor of 2.
- (ii) We expect shot noise to dominate any dipole in the 87GB-PMN catalogues.
- (iii) When we measure the dipole we find that,
 - For no correction of the catalogues, A is 3.5σ above the noise, but over 50° away from the LG-CMB dipole.

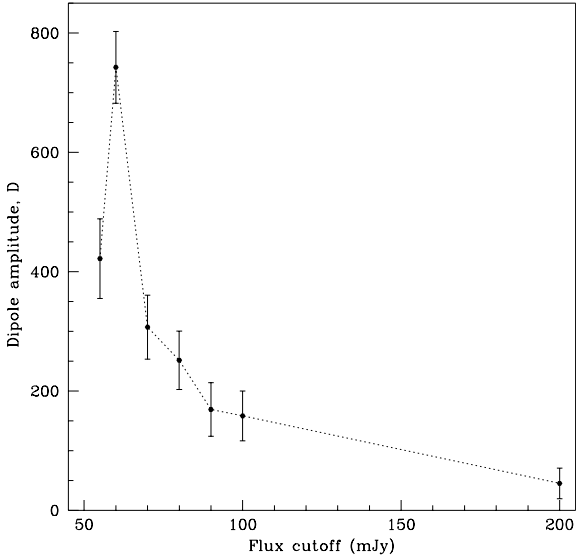


Figure 4. After \mathcal{N} matching : Detected dipole amplitude, D , for flux cutoffs from 50 mJy to 200 mJy.

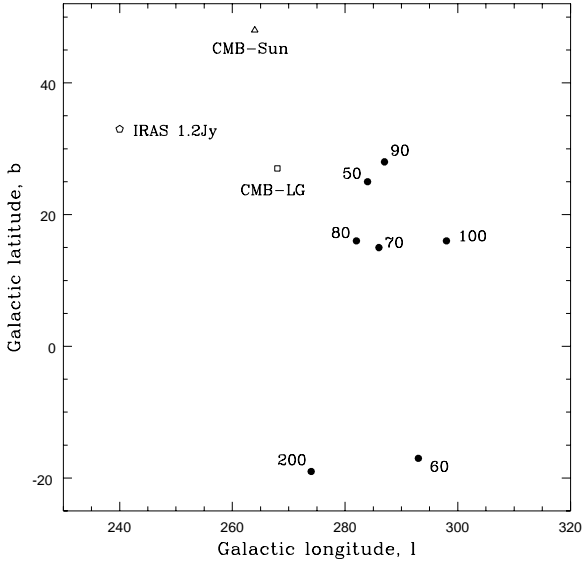


Figure 5. After \mathcal{N} matching : Detected dipole direction, for flux cutoffs from 50 mJy to 200 mJy (filled circles), the IRAS 1.2 Jy dipole (open pentagon), LG-CMB dipole (open square), and Sun-CMB dipole (open triangle).

- When we try the flux matching procedure, we measure a dipole signal of only 0.5σ above noise, but now the dipole points 20° away from the LG-CMB dipole.

We attribute most of the initially measured dipole signal to the fact that two different reduction algorithms were used in compiling the 87GB-PMN catalogues. The signal decreases after flux matching, but is still above shot noise level. In addition, we now see closer alignment with the LG-

CMB dipole, that we should not detect a priori. What might produce these effects?

We hope that, after the flux matching done, the 87GB – PMN_{match} catalogue is consistent, and not producing additional significant dipole effects, resulting from the slight, remaining \mathcal{N} mismatch. However, as mentioned, there is the possibility that survey geometry is significantly influencing the dipole alignment.

An alternate explanation of the dipole detection over what we predict, could come from the large scale structure prediction. The large scale structure dipole we predict is for an ensemble average of observers over a universe (with LDCDM power spectrum). The dipole measurement of the 87GB-PMN catalogue represents only one realization, which may greatly differ from the ensemble average. We may live in a highly non-homogeneous part of the universe. There is the possibility that we are detecting real large scale structure. As we report in Section 7 we detect a slight increase in the mean density of sources in the 87GB_{raw} and PMN_{raw} catalogues within $10^\circ - 15^\circ$ along the Super Galactic Plane. This structure may contribute to the remaining dipole signal we measure.

Some support for a dipole pattern in the distribution of radio galaxies comes from an analysis by Lahav & Shaver (1991, unpublished). They analysed an optically-radio selected sample (Shaver 1991) of 92 galaxies which flux at 408 MHz larger than 1 Jy and blue magnitude brighter than 14.5, 2/3 of them with redshift $z < 0.02$. If the dipole is so local, it is due to only few hundreds of sources (see our discussion of the SGP below).

6 SHA APPLICATION

We now compare observations and predictions for higher harmonics. The fluctuations in radio sources can be related to the fluctuations in mass via the linear bias parameter b_R , as $\sigma_{8,R} = b_R \sigma_{8,M}$. The models we use for our predictions are for a universe with $\Omega = 1$ geometry, but we allow 2 possible power-spectra: (i) standard CDM power spectrum with $\Omega = 1.0$, $h = 0.5$, and normalization specified by the rms fluctuations in radio counts in $8 h^{-1}$ Mpc spheres, $\sigma_{8,R} = 1.0$ and (ii) a power spectrum parameterised as an unbiased ($\sigma_{8,R} = 1.0$) low density CDM (LDCDM) spectrum shape parameter $\Gamma = 0.2$ (Bardeen et al. 1986).

We can rewrite the corrected harmonic coefficients as

$$C_l^2 = \frac{1}{\mathcal{N}(\Omega_{obs}/4\pi)(2l+1)} \sum_m |c_l^m|_{tot}^2 = 1 + \frac{\langle |c_l^m|^2 \rangle_{mod}}{\mathcal{N}(\Omega_{obs}/4\pi)} \quad (34)$$

for $|c_l^m|_{tot}^2$ being the predicted harmonics (signal+noise, for an incomplete sky) or the observed harmonics. Subsequently, C_l tells us directly how many standard deviations above the shot noise a measurement or prediction is. The predicted harmonic in the absence of noise $\langle |c_l^m|^2 \rangle_{mod}$ and C_l (including noise) for a flux cutoff of 70mJy and both power spectra are listed in Table 5. Incomplete sky coverage has been corrected for, according to eqn. 19.

The models predict (see Table 5) that due to our observing constraints, we will not see much power (if large scale structure exists in CDM or LDCDM form) over shot noise for any order l . The shot noise level is at $C_l = 1$. However, we have already measured a larger than predicted

Table 5. The predicted harmonic coefficients for CDM and LDCDM models for a flux limit of 70 mJy, for $l = 1$ to $l = 5$.

CDM		LDCDM		
1	$\langle c_l^m ^2 \rangle_{mod}$	C_l	$\langle c_l^m ^2 \rangle_{mod}$	C_l
1	16.4	1.0040	50.7	1.0120
2	17.3	1.0042	47.3	1.0116
3	17.5	1.0043	43.6	1.0106
4	17.0	1.0042	39.6	1.0096
5	16.5	1.0040	36.4	1.0088

dipole amplitude in the $87GB - PMN_{match}$ data, so we are interested in what the data harmonics will show.

Before \mathcal{N} matching, for the 87GB-PMN catalogue, we see a large dipole ($l = 1$) and significant signal in harmonics up to $l = 10$. The $87GB - PMN_{match}$ data show amplitudes somewhat reduced (mainly for the lower harmonics $l < 6$, but they are still far above the predicted amplitudes. Even for a full sky, filled to the same mean density as for the 70mJy flux matched case, the harmonic coefficients oscillate considerably around the shot noise prediction. It is also interesting to note that the flux matched data harmonics have higher overall amplitudes the lower the flux cutoff, following the general trend predicted in the models.

Figure 6 shows the harmonics for the $87GB - PMN_{match}$ catalogue with a 70mJy flux cutoff, compared to the predicted harmonics for the same flux cutoff, corrected for the incomplete sky coverage. For the model prediction, we plot the resulting C_l 's for $\langle |c_l^m|^2 \rangle_{mod} \times 1, \times 15, \times 30$, and $\times 45$, and can see that the galaxy harmonics are consistent with being about a factor of 15 to 30 above the prediction (including shot noise).

The above predictions for the radio harmonics assume no biasing, i.e. the normalization is fixed to $\sigma_{8,R} = b_R \sigma_{8,M} = 1$. If we interpret the observed, \mathcal{N} matched harmonics as being real, we can use them to estimate the amplitude $\sigma_{8,R}$ for a given shape of the power-spectrum. For example, for the quadrupole ($l = 2$) and flux limit of 70 mJy the observation $C_2 \sim 1.3$ can be made to agree with the CDM and LDCDM predictions if $\sigma_{8,R} \sim 9$ and ~ 5 respectively. (With better data one should estimate the normalisation using Maximum Likelihood, e.g. Scharf et al. 1992; Fisher et al. 1994.) These crude results suggest a very high bias parameter b_R , but in qualitative agreement with the measurement of high correlation length for radio sources. For example, for 87GB and PMN at redshift $z = 0$, $\xi(r) = (r/r_0)^{-1.8}$ with $r_0 = 18h^{-1}$ Mpc (Loan et al. 1997), assuming stable clustering. This can be translated (Peebles 1980) to $\sigma_{8,R} \approx \sqrt{1.86(r_0/8)^{1.8}} \sim 2.8$.

Figure 2 shows (solid triangle and circle) the estimates of the power-spectrum at $k^{-1} \sim 600h^{-1}$ Mpc, assuming the shape of standard CDM and LDCDM power-spectra respectively. They are based on the measured quadrupole from the combined 70 mJy $87GB - PMN_{match}$ sample. Given the problems of catalogue matching and shot-noise, these points should be interpreted at best as ‘representative upper limits’, not as detections.

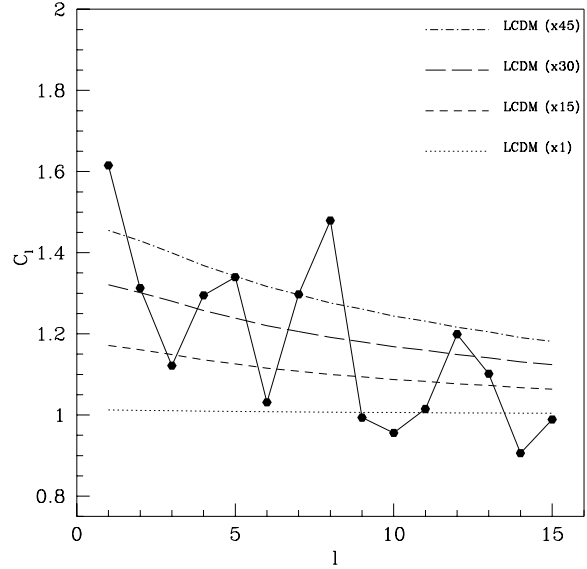


Figure 6. C_l comparison for $87GB - PMN_{match}$ 70mJy data and LDCDM model predictions ($\langle |c_l^m|^2 \rangle_{mod} \times 1, \times 15, \times 30$ and $\times 45$). The dots connected by a solid line indicate the data harmonics, while the various dashed and dotted lines indicate the model harmonics. $C_l = 1$ is the shot noise level.

7 THE SUPERGALACTIC PLANE (SGP)

The large-area uniformity of the 87GB-PMN surveys was adopted as the criterion for a sensible choice for sky mask and flux-density limit. This produced the masked catalogue used to calculate the dipole and higher harmonics in this study, as well as the angular correlation function in Loan et al. (1997). Nevertheless, nearby structures, such as the Supergalactic Plane (SGP), may introduce detectable inhomogeneities into the catalogues on large angular scales.

The SGP is an over-dense region of the local universe. William Herschel was the first to note that ‘nebulae’ seemed to be more concentrated in a band across the heavens. More recently, the Virgo cluster was seen as the centre of a ‘metagalaxy’ or ‘Local Supercluster’. De Vaucouleurs (1975) recognized a great circle along which there was an increased density of galaxies in the Shapley-Ames optical galaxy catalogue. This great circle defines a system of Supergalactic spherical coordinates, in which the SGP lies along the equator and the north pole lies at Galactic coordinates ($\ell = 47.37^\circ$, $b = 6.32^\circ$). The SGP is readily apparent as a region of greatly enhanced surface density of galaxies in more recent large-area surveys of nearby optical galaxies (e.g. Lynden-Bell & Lahav 1988). Although the SGP seems to be a local phenomenon, perhaps analogous to the sheets and filaments discovered by galaxy surveys, it is not clear where it ends. Studies of the SGP using the IRAS 1.2 Jy and ORS surveys (Lahav et al., in preparation) show that the SGP is not a simple planar structure.

7.1 Histograms approach

In the case of full sky coverage, the great circle along which the density of galaxies is enhanced can be found by calculat-

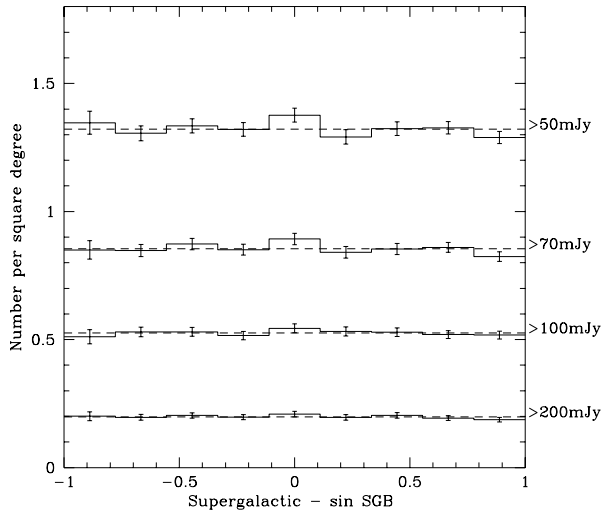


Figure 7. Source surface density of $87GB_{raw}$, as a function of SGB and flux-density limit. Error bars are Poissonian. The 9 bins are evenly spaced in $\sin(SGB)$. The area of each bin is estimated by Monte Carlo integration. The dotted line shows the mean source density over the whole survey.

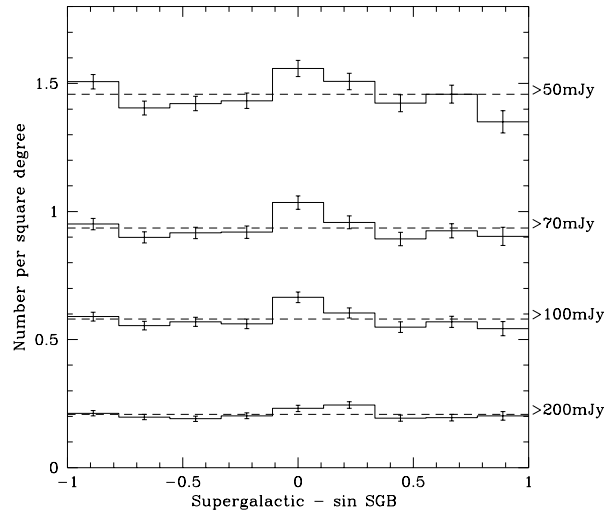


Figure 8. Source surface density of PMN_{raw} , as a function of SGB and flux-density limit. Error bars are Poissonian. The 9 bins are evenly spaced in $\sin(SGB)$. The area of each bin is estimated by Monte Carlo integration. The dotted line shows the mean source density over the whole survey.

ing the ‘moment of inertia’ (Webster, Lahav & Fisher 1997; Lahav et al., in preparation). This approach is obviously only valid for a uniformly-selected catalogue with full sky coverage, which unfortunately is not the case here. Moreover, clusters and voids outside the ‘plane’ may confuse the analysis as well. We prefer instead a more direct approach, where each catalogue ($87GB_{raw}$ and PMN_{raw}) is analysed independently by histograms of number counts.

In order to explore whether the SGP is indeed visible in the $87GB_{raw}$ and PMN_{raw} catalogues, we now calculate the surface density of sources as a function of position in Equatorial (α, δ), Galactic (l, b) and Supergalactic (SGL, SGB) coordinate systems. The $87GB_{raw}$ and PMN_{raw} catalogues are treated here separately, to avoid being misled by the flux-density miscalibration highlighted earlier. In the study of the SGP we use the more conservative flux limit of 100 mJy.

In Supergalactic coordinates, the sky is divided into strips of roughly equal area, equally spaced in $\sin(SGB)$ and covering the full range of SGL . The density of sources in each strip is found by adding up the number of sources in each catalogue within each strip, and dividing by the masked area of the strip (that is, the area of the strip inside the mask for each catalogue). The total area of a strip may be easily calculated using spherical geometry, but this simple calculation is complicated by the numerous parts of the sky that are excluded from the analysis by the choice of the mask. Instead, the area of each strip within the mask is estimated by Monte Carlo integration. Many points are put down at random positions within each strip, and the number of points included within the masked area is calculated. Thus, the area of each strip is the ratio of included random points to the total number of random points, multiplied by the total (un-

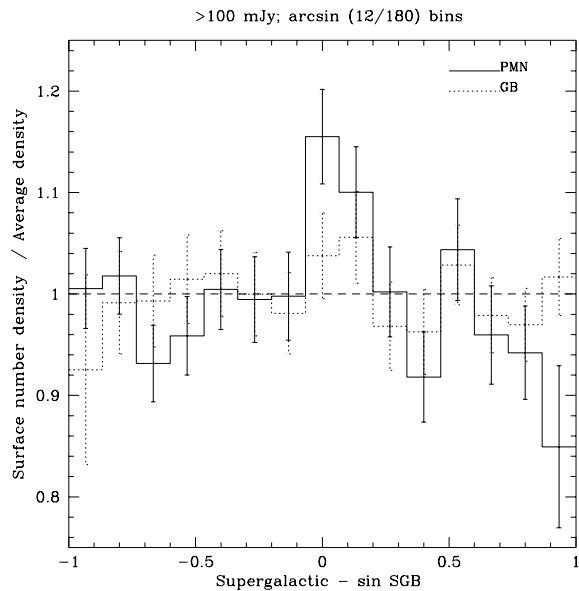


Figure 9. Surface density of sources above 100mJy in the $87GB_{raw}$ and PMN_{raw} catalogues, as a function of SGB . Error bars are Poissonian. The 15 bins are evenly spaced in $\sin(SGB)$. The area of each bin is estimated by Monte Carlo integration. Results for each catalogue are calculated separately, and normalized by the average number density in that catalogue.

masked) area of the strip. This estimate of the area is found to be accurate to within a small fraction of 1 per cent.

Figures 7 and 8 show how the number of sources in the $87GB_{raw}$ and PMN_{raw} catalogues changes with the flux-density limit and as a function of SGB . Both catalogues appear to be complete above 50 mJy, but display incompleteness at the 35 mJy limit (not shown). The $87GB_{raw}$ plot, Figure 7, is consistent with a uniform distribution at all flux limits, although there is a suggestion of a small excess near $SGB = 0^\circ$. The PMN_{raw} plot, Figure 8, displays a strong density enhancement near the Supergalactic equator ($SGB = 0^\circ$) at all complete flux limits.

Figure 9 shows how the surface density of sources above a flux-density limit of 100 mJy varies as a function of SGB in the $87GB_{raw}$ and PMN_{raw} catalogues. There is a significant increase in source surface density close to the SGP in the PMN_{raw} catalogue, but any increase is not statistically significant in the $87GB_{raw}$ catalogue. Replotting this histogram for a different binning scheme retained this excess around the SGP, indicating that these results are not sensitive to the choice of bin size. Tables 6 and 7 quantify the excess density within the central strip (either side of $SGP = 0^\circ$) for the $87GB_{raw}$ and PMN_{raw} catalogues, respectively. Approximately 70% of the SGP in each hemisphere is included in the central strip. Repeating this analysis with strips of finite width in SGL , both for the whole range of SGB and also for sources within 10° of the SGP, shows that no single cluster of sources causes this increase, but that the over-density close to the SGP is distributed along the Supergalactic equator.

A similar procedure was followed in Equatorial coordinates, plotting similar histograms with bins equally spaced in $\sin(\delta)$ and covering the whole range of α . It is clear that $87GB_{raw}$ and PMN_{raw} have slightly different flux calibrations, in accord with the discussion earlier. Even far above the published flux-density limits of both surveys (~ 50 mJy) there are more sources per unit area above a given flux limit in PMN_{raw} than there are in $87GB_{raw}$. Fortunately, since both surveys are analysed separately, this problem will not affect these results. However, it does mean that the flux limits given here are somewhat different from the real flux limits. This difference will not greatly affect the generally observed trend, because the radio luminosity function is so broad. There is also the possibility of biases caused by ignoring sources which lie just below the flux limit through experimental error in the surveys. Apart from the disturbing flux mismatch highlighted here, no significant density enhancements are seen in Equatorial coordinates.

No significant patches of increased surface density are seen when a similar analysis is performed in Galactic coordinates (ℓ, b) , plotting histograms of bins equally spaced in $\sin(b)$. Failure to detect any increase in source surface density close to the Galactic Plane shows that there is very little contamination from Galactic sources.

Similar analyses were conducted, binning the sources in bins of equal width in right ascension (α), Galactic longitude (ℓ) and Supergalactic longitude (SGB). Again, no significant departures from the mean sources density were observed.

7.2 Comparison with previous studies

The PMN_{raw} survey shows a significant enhancement of the radio source surface density within $\sim 10^\circ$ of the Supergalactic Plane: an increase of $\sim 15\%$ compared to the mean value. This is good evidence for concentration of radio sources towards the SGP, although it is puzzling that there is no corresponding over-density in the northern sky. The concentration of low-Supergalactic-latitude sources in PMN_{raw} is not due to one cluster of sources, but rather it is spread along the whole SGP. The number of sources necessary to create this enhancement is quite small (~ 200).

The tests for increased numbers of radio sources close to the SGP follows a similar analysis of the Molonglo 408 MHz survey of the southern hemisphere (Shaver & Pierre 1989). Shaver & Pierre found a significant increase in the surface density of sources close to the SGP. This work confirms the presence of significant concentration of radio sources within 10° of the standard SGP equator in the southern hemisphere (PMN_{raw}), but this is not mirrored in the north ($87GB_{raw}$). Shaver (1991) pointed out that there may be an asymmetry in the SGL-distribution of the radio galaxies (in the Great Attractor direction), and this would explain the fact that the SG concentration is more evident in the southern hemisphere than in the north. Shaver & Pierre (1989) also analysed a small redshift survey, finding that there was a significant preference for nearby ($z < 0.02$) radio sources to lie close to the SGP, but that this preference was not observed for radio sources at higher redshift ($0.02 < z < 0.1$).

The present analysis finds an over-density of about 130 radio sources with a 4.85 GHz flux density above 100 mJy within an area of about 1500 square degrees, up to 10° either side of the SGP in the southern hemisphere. A less significant over-density is also observed in the north. The models of Dunlop & Peacock (1990) predict that the surface density of radio sources above 100 mJy within a redshift $z < 0.02$ is ≈ 18 per str (1 str = 3282.97 square degrees). It is interesting to note that the over-density found along the SGP in the PMN_{raw} survey could be accounted for by approximately the same number of radio sources found within a redshift $z < 0.02$ ($\sim 60h^{-1}$ Mpc).

If we assume that the over-density in the PMN_{raw} survey is caused by nearby radio galaxies out to a redshift $z = 0.02$, then we can estimate the thickness of SGP. The angle subtended by the over-dense strip is $\theta \sim 20^\circ$, and thus, at the distance corresponding to $z = 0.02$ ($d = cz/H_0 = 60h^{-1}$ Mpc), the SGP has a thickness $\sim 2d \tan(\theta/2) \approx 20h^{-1}$ Mpc. This also raises the question of how far the SGP extends. One test of the hypothesis that the over-density close to the SGP really is caused by nearby radio sources would be to cross-correlate the radio sources with those in the optical IRAS catalogues, in a similar way to the study by Shaver (1991).

It may be possible to cross-identify objects that are both optical IRAS sources and also radio sources in the $87GB_{raw}$ and PMN_{raw} catalogues. Repeating this analysis after removing radio sources that appear in the optical and IRAS catalogues may show whether the apparent over-density close to the SGP is caused by a flattened distribution of nearby sources.

It could be argued that these results may be pure statistical fluke, and that the detected over-density is caused

Table 6. Excess number of radio sources close to the SGP for $87GB_{raw}$, above 100 mJy. Total number = 8272, Area = 15732 deg², mean density = 0.526 deg⁻². The number expected (\bar{N}) is calculated from the mean density. The distance from the mean is the number of standard deviations ($\sqrt{\bar{N}}$) that the detected source excess ($N - \bar{N}$) lies from the expected number. Note that the mean density is an over-estimate since it includes any over-density close to the SGP. Thus, the distance from the mean is under-estimated.

Central bin width (deg)	Bin area (deg ²)	# found (N)	# expected (\bar{N})	# excess ($N - \bar{N}$)	Distance from mean ($(N - \bar{N})/\sqrt{\bar{N}}$)
±3.82	1103	602	580	22	0.9
±6.38	1819	989	956	33	1.0
±11.54	3237	1741	1702	39	0.9
±19.47	5335	2828	2805	23	0.4

Table 7. Excess number of radio sources close to the SGP for PMN_{raw} , above 100 mJy. Total number = 7829, total area = 13486 deg², mean density = 0.581 deg⁻².

Central bin width (deg)	Bin area (deg ²)	# found (N)	# expected (\bar{N})	# excess ($N - \bar{N}$)	Distance from mean ($(N - \bar{N})/\sqrt{\bar{N}}$)
±3.82	914	613	531	82	3.3
±6.38	1534	1020	891	129	4.1
±11.54	2766	1742	1606	136	3.3
±19.47	4604	2807	2673	134	2.5

by a relatively small number of radio sources. However, it is not clear how a bias towards detecting sources that lie close to the SGP could have entered the radio surveys.

On large angular scales, there is a clear detection of the SGP in the southern sky, but not in the north. The over-density in the south may be attributed to nearby radio galaxies lying preferentially toward the SGP, but it is not clear why there is no significant detection in the north. Possible explanations of this conundrum include the possibilities that nearby sources are somehow excluded from $87GB_{raw}$, or that they are counted more than once in PMN_{raw} (e.g. nearby double-lobed radio sources may be included twice). Cross-identification of sources in the radio surveys with optical and IRAS galaxies (both relatively shallow surveys, out to ≈ 6000 km/s) could be used to find the nearby radio sources, to check if they are indeed responsible for the over-density close to the SGP.

8 DISCUSSION

We have studied in this paper the possibility of using radio surveys with median redshift $z \sim 1$ to probe large scale structure. In particular, we have utilised the technique of spherical harmonics to predict the amplitude of the dipole and higher in the angular distribution of radio galaxies.

Our conclusions are:

(a) The dipole is due to 2 effects which turn out to be of comparable magnitude: (i) our motion with respect to the CMB, and (ii) large scale structure,

(b) Catalogues like $87GB$ and PMN have the potential

of probing structure on large scales, e.g. The quadrupole measures scales of $k^{-1} \sim 600h^{-1}$ Mpc.

(c) Unfortunately, the Poisson shot noise in these sparse catalogues is expected to be large than the clustering signals, as predicted for a family of Cold Dark Matter models.

(d) However, we detect dipole and higher harmonics in the combined $87GB - PMN_{raw}$ catalogue which are far larger than expected. We attribute this to a 2% flux mismatch between the two catalogues. Ad-hoc corrections to match the catalogues may suggest a marginal detection of a dipole.

There are two likely explanations for this. One is that we are still seeing the effect of survey geometry, or incompatibility of data reduction algorithms in producing the catalogues. The second is that, because the catalogues represent only one realization of the ensemble average harmonics we predict, we may be detecting local structure that causes the large amplitude we measure.

(e) To detect a dipole and higher harmonics unambiguously, a catalogue with full sky coverage and $\sim 10^6$ sources is required.

(f) We have investigated the existence and extent of the Supergalactic Plane in the above catalogues. In a strip of $\pm 10^\circ$ of the standard Supergalactic equator we find a 3σ detection in PMN_{raw} , but only 1σ in $87GB_{raw}$. This analysis demonstrates that large-scale structure studies based on new radio surveys nearing completion will provide important estimates of distant structure and its evolution. On-going surveys with the VLA, FIRST (Becker, White & Helfand 1995) and NVSS (Condon 1997), will yield approximately 10^6 sources over the sky, thus overcoming the limitations imposed by the shot-noise at the current 4.85 GHz surveys.

Furthermore, the positional accuracy of these new surveys will be sufficient for optical spectroscopy using candidates directly from the catalogues. Although difficult to obtain, redshifts to the radio sources are essential in order to improve the measurement of the power-spectrum by localizing the clustering pattern in 3 dimensions.

Acknowledgements: We thank A. Fabian, E. Gawiser, M. Hudson, A. Heavens, A. Lasenby, T. Piran, M. Rees, C. Scharf, P. Shaver, M. Treyer, M. Webster and K. Wu for helpful discussions and comments. AB was supported by a Winston Churchill Scholarship and a NSF Graduate Fellowship. AJL acknowledges the receipt of a PPARC studentship.

REFERENCES

- Bardeen J.M., Bond J.R., Kaiser N., Szalay A., 1986, *ApJ*, 304, 15
- Baugh C.M., Efstathiou G., 1993, *MNRAS*, 265, 145
- Baugh C.M., Efstathiou G., 1994, *MNRAS*, 267, 323
- Becker R.H., White R.L., Helfand D.J., 1995, *ApJ*, 450, 559
- Benn C.R., Wall J.V., 1995, *MNRAS*, 272, 678
- Condon J.J., 1997, in Mclean et al. eds, *Proc. IAU Symp.* 179, Multi-wavelength sky surveys, Kluwer
- Condon J.J., Broderick J.J., Seielstad, G.A., 1989, *AJ*, 97, 1064
- Cress C.M., Helfand D.J., Becker R.H., Gregg, M.D., White, R.L., 1996, *ApJ*, 473, 7
- de Vaucouleurs G. 1975, *ApJ*, 202, 610
- Dunlop J.S., Peacock J.A., 1990, *MNRAS*, 247, 19
- Ellis G.F.R., Baldwin J.E., 1984, *MNRAS*, 206, 377
- Fisher K.B., Scharf C.A., Lahav O., 1994, *MNRAS*, 266, 219
- Fisher K.B., Lahav O., Hoffman Y., Zaroubi S., Lynden-Bell D., 1995, *MNRAS*, 272, 885
- Fisher K.B., Huchra J.P., Davis M., Yahil A., Schlegel D., 1995, *ApJS*, 100, 69
- Gregory P.C., Condon J.J., 1991, *ApJS*, 75, 1011
- Gregory P.C., Vavasour J.D., Scott W.K., Condon J.J., 1994, *ApJS*, 90, 173
- Griffith M.R., Wright A.E., 1993, *AJ*, 105, 1666
- Griffith M.R., Wright A.E., Burke B.F., 1995, *ApJS*, 97, 347
- Griffith M.R., Wright A.E., Burke B.F., Ekers R.D., 1994, *ApJS*, 90, 179
- Harmon R.T., Lahav O., Meurs E.J.A., 1987, *MNRAS*, 228, 5p
- Heavens A.F., Taylor A.N., 1995, *MNRAS*, 275, 483
- Hudson M., 1993, *MNRAS*, 265, 72
- Kaiser N., 1984, *ApJ*, 284, L9
- Kaiser N., Lahav O., 1989, *MNRAS*, 237, 129
- Kooiman L.K., Burns J.O., Klypin A.A., 1995, *ApJ*, 448, 500
- Lahav O., 1987, *MNRAS*, 225, 213
- Lahav O., 1994, in Bouchet et al. eds, *Cosmic Velocity Fields*, Paris, p.205
- Lahav O., Rowan-Robinson M., Lynden-Bell D., 1988, *MNRAS*, 234, 677
- Lahav O., Piran T., Treyer M.A., 1997, *MNRAS*, 284, 499
- Loan A.J., Wall J.V., Lahav O., 1997, *MNRAS*, 286, 994
- Lynden-Bell D., Lahav O. 1989, in Coyne G., Rubin V. C., eds, *Proc. of the Vatican Study Week*, Princeton University Press, Princeton
- Lynden-Bell D., Lahav O., Burstein D., 1989, *MNRAS*, 241, 325
- Meiksin A., Davis M., 1986, *AJ*, 91, 191
- Nusser A., Davis M., 1994, *ApJ*, 421, L1
- Peebles P.J.E., 1973, *ApJ*, 185, 413
- Peebles P.J.E., 1980, *The Large Scale Structure of the Universe*. Princeton Univ. Press, New Jersey
- Piran T., Singh A., 1996, *astro-ph/9607072*
- Plionis M., 1988, *MNRAS*, 234, 401
- Rowan-Robinson M., Saunders W., Lawrence A., Leech K.L., 1991, *MNRAS*, 253, 485
- Scharf C., Lahav O., 1993, *MNRAS*, 264, 439
- Scharf C., Hoffman Y., Lahav O., Lynden-Bell D., 1992, *MNRAS*, 256, 299
- Shaver P.A., 1991, *Aust. J. Phys.*, 44, 759
- Shaver P.A., Pierre M., 1989, *A&A*, 220, 35
- Sicotte H., 1995. PhD thesis, Princeton University
- Smoot G.F., Bennett C.L., Kogut A., Wright E.L., Aymon J., Boggess N.W., Cheng E.S., De Amici G., Gulkis S., Hauser M.G., 1992, *ApJ*, 396, L1
- Strauss M.A., Willick J.A., 1995, *Phys. Rep.*, 261, 271
- Strauss M.A., Yahil A., Davis M., Huchra J.P., Fisher K.B., 1992, *ApJ*, 397, 395
- Villumsen J.V., Strauss M.A., 1987, *ApJ*, 322, 37
- Webster A., 1976, *MNRAS*, 175, 61
- Webster A.M., Lahav O., Fisher K.B., 1997, *MNRAS*, 287, 425
- Wright A.E., Griffith M.R., Burke B.F. & Ekers R.D., 1994, *ApJS*, 91, 111
- Wright A.E., Griffith M.R., Hunt A.J., Troupe E., Burke B.F., Ekers R.D., 1996, *ApJS*, 103, 145
- Yahil A., Walker D., Rowan-Robinson M., 1986, *ApJ*, 301, L1
- Zare R.N., 1987, *Angular Momentum - Understanding Spatial Aspects in Chemistry and Physics*. John Wiley & Sons, New York